

A Geometric Analysis of Small-sized Language Model Hallucinations

Emanuele Ricco¹ Elia Onofri^{1,2} Lorenzo Cima^{3,4} Stefano Cresci³ Roberto Di Pietro¹

Abstract

Hallucinations—fluent but factually incorrect responses—pose a major challenge to the reliability of language models, especially in multi-step or agentic settings.

This work investigates hallucinations in small-sized LLMs through a geometric perspective, starting from the hypothesis that when models generate multiple responses to the same prompt, genuine ones exhibit tighter clustering in the embedding space, we prove this hypothesis and, leveraging this geometrical insight, we also show that it is possible to achieve a consistent level of separability. This latter result is used to introduce a label-efficient propagation method that classifies large collections of responses from just 30–50 annotations, achieving F1 scores above 90%.

Our findings, framing hallucinations from a geometric perspective in the embedding space, complement traditional knowledge-centric and single-response evaluation paradigms, paving the way for further research.

1. Introduction

Language models are now extensively deployed across a wide range of applications, including information retrieval, content generation, decision support, and interactive systems. Alongside large, resource-intensive models accessible primarily to well-resourced organisations, *small-sized language models* have gained increasing adoption due to their efficiency, deployability, and transparency (Wu et al., 2025). Advances in scaling laws and training strategies have further narrowed the performance gap between small models and earlier generations of much larger systems (Chung et al., 2024), making them attractive in practical pipelines and

¹King-Abdullah University of Science and Technology (KAUST), CEMSE division, Thuwal, Saudi Arabia ²Institute for Applied Mathematics, National Research Council (IAC-CNR), Italy ³IIT-CNR, Pisa, Italy ⁴University of Pisa, Department of Information Engineering, Pisa, Italy. Correspondence to: Emanuele Ricco <emanuele.ricco@kaust.edu.sa>.

Preprint. February 17, 2026.

agentic architectures (Belcak et al., 2025). In such settings, reliability becomes critical: incorrect or fabricated responses can propagate through multi-step reasoning chains or coordinated agents, amplifying their impact (Hao et al., 2024).

A central obstacle to reliability is the generation of responses that appear fluent and plausible while being factually incorrect, commonly referred to as *hallucinations* (Huang et al., 2023; Ji et al., 2023; Li et al., 2023). Much of the existing literature frames hallucinations as a consequence of missing or inaccessible knowledge, often attributing incorrect generations to limitations in training data coverage, probabilistic decoding, or noise in internal representations (Lin et al., 2022; Xu et al., 2024; Kalai et al., 2025). As a result, substantial effort has focused on hallucination detection and evaluation, typically treating each prompt–response pair individually while asking if the model “knows” the correct answer (Farquhar et al., 2024; Niu et al., 2025; Su et al., 2024; Tonmoy et al., 2024).

However, this single-response perspective obscures an important empirical observation: for many prompts, the same model can generate both correct and incorrect answers across repeated samplings. In such cases, the relevant factual knowledge is demonstrably present, yet generation might diverge toward incorrect outcomes. This suggests an alternative interpretation where hallucinations are not primarily driven by absence of knowledge, but by failures in how available information is retrieved and instantiated at generation. From this perspective, hallucinations emerge not as isolated errors, but as part of a broader *structural organisation* of responses produced under the same prompt.

In this work, we adopt this alternative viewpoint and study hallucinations through a geometric analysis of repeated model responses. Rather than analysing internal model states or the generation process itself, we focus on the *emerging relations within the space spanned by the embeddings of responses*: we embed multiple generations obtained under the same prompt and examine the distributional structure formed by genuine and hallucinated answers. We restrict attention to prompts for which models produce multiple factually correct responses, ensuring that the analysis isolates hallucinations arising under conditions where the required knowledge is demonstrably available. Under this assumption, divergence across generations can be interpreted as

a retrieval instability (or instantiation-level phenomenon) rather than a persistent misconception.

Our analysis reveals that genuine and hallucinated responses exhibit systematically different geometric properties in embedding space, with hallucinated responses displaying reduced semantic cohesion relative to genuine ones. These structural differences are stable across models, prompts, and class balances, and cannot be explained by sampling artefacts alone. Moreover, we show that this geometry can be exploited to propagate labels from a small set of judged responses to large collections of prompt-consistent generations, enabling accurate and label-efficient classification.

Taken together, our results suggest that hallucinations in small-sized LLMs can be effectively detected as a geometric phenomenon arising from retrieval instability, rather than solely as a lack of knowledge. This shift in perspective complements existing detection-focused approaches and highlights the value of analysing hallucinations at the level of response distributions rather than individual generations.

Contributions

- (i) We formulate and validate the hypothesis that hallucinated responses arising under conditions of available factual knowledge exhibit, in the embedding space, weaker semantic cohesion than non hallucinated ones—displaying distinctive and stable geometric signatures.
- (ii) We show that leveraging the above introduced geometric interpretation, it is possible to achieve strong distributional separability between genuine and hallucinated responses.
- (iii) We leverage the cited separability to introduce a scalable, geometry-aware label propagation framework which transfers hallucination tagging from a small set of judged responses to large collections of prompt-consistent generations, achieving F1 scores above 90%.
- (iv) We release a fully labeled dataset of repeated responses (150 generations for 200 prompts across 10 small-sized LLMs) to support structural analyses of hallucinations.

Roadmap The next section reviews related work; Section 3 introduces the adopted methodology; Section 4 reports the achieved results, while their discussion is in Section 5; and, finally, Section 6 sports some concluding remarks.

2. Related Work

Small-sized LLMs (7–30B) offer practical advantages in terms of efficiency, deployability, and accessibility, enabling fast inference and domain-specific customization. However, these benefits raise important concerns about reliability and trustworthiness, particularly regarding hallucinations, which motivate the need for systematic analysis and detection

strategies (Bang et al., 2025).

Trustworthiness in Small Language Models Trustworthiness in language models is often discussed in terms of factual accuracy, calibration, and reliability under uncertainty. TrustLLM is a relevant framework in this field (Huang et al., 2024), establishing eight trustworthiness dimensions, including truthfulness, safety, and robustness, and evaluating them across 16 models and 30+ datasets. Trustworthiness is a broad term encompassing safety (Qi et al., 2025), alignment (Ouyang et al., 2022), and ethical considerations (Bender et al., 2021), with recent work focusing on empirical evaluation frameworks (Chafekar et al., 2024). Factuality evaluation benchmarks provide a standardized assessment of truthfulness across diverse scenarios. FactBench (Bayat et al., 2025) introduces a benchmark with 1K prompts spanning 150 topics, revealing that factuality does not necessarily improve with scale. The FACTS Leaderboard (Jacovi et al., 2025) evaluates language models’ ability to generate factually accurate responses in information-seeking scenarios. FactScore (Min et al., 2023) decomposes long-form generations into atomic facts supported by reliable sources, while Ling et al. (2024) investigates trustworthiness of LLMs associated with in-context learning. Beyond individual response accuracy, recent work has identified systematic homogeneity in model outputs, with over 70% similarity observed on different models (Jiang et al., 2025).

Hallucination Detection Recent advances in hallucination detection exploit internal model representations rather than relying solely on output-level analysis. Sriramanan et al. (2024) investigates LLM internal states while Han et al. (2024) explores neuron-level mechanisms identifying specific activation patterns correlated with hallucination behavior. Building on these approaches, Bar-Shalom et al. (2025) designed a Vision Transformer-inspired model while Niu et al. (2025) proposed a methodology based on critical token selection from a response. Internal states have been widely studied by Su et al. (2024) with an unsupervised training framework leveraging internal states of LLMs for real-time hallucination detection. Together with internal representations, semantic-level approaches analyze the meaning and consistency of responses. Farquhar et al. (2024) proposed entropy-based uncertainty estimators to detect confabulations while Manakul et al. (2023) introduced SelfCheckGPT, manually annotating factuality in GPT-3 generated passages across multiple samples. Overall, most existing work treats hallucinated responses as a consequence of missing or incorrect knowledge. In contrast, our work focuses on questions for which the model demonstrably possesses the relevant knowledge and investigates the structural patterns in representation space that nonetheless lead to hallucinated generations.

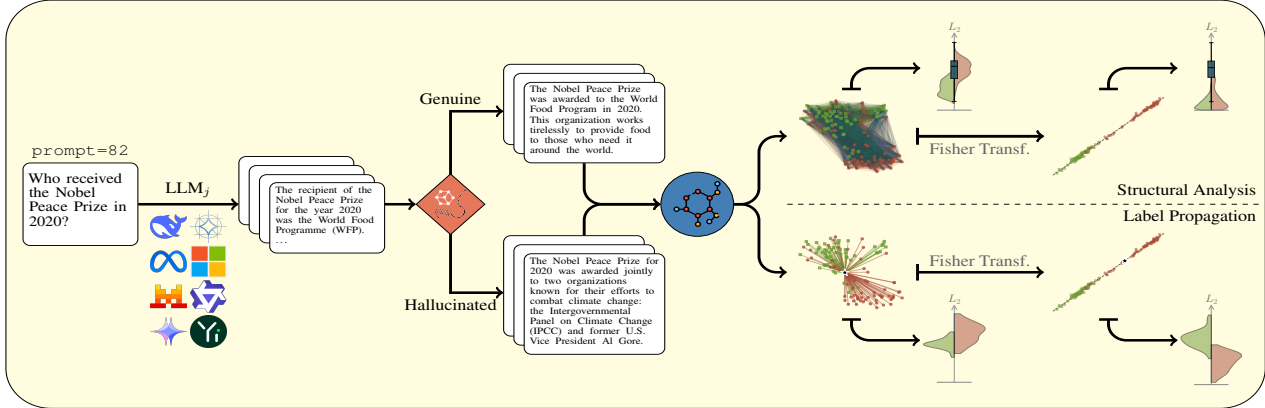


Figure 1. Pipeline of the proposed method. (Left) 200 different prompts are fed into 10 LLMs, generating 150 responses each. (Center) Responses are tagged as Genuine (G, green) or Hallucinated (H, red) under Claude Sonnet 4.5, and embedded through SBERT (blue circle) in \mathbb{R}^{384} (here reduced with T-SNE for plots). Two analyses follow. (*Structural*, top right) Mutual distances intra-G, intra-H, and inter-(GH) (blue) are evaluated in the embedding space, showing significant differences in the distributions (cf. Figures 2 and 3), yet being non directly separable; data points are embedded into the linear space maximising Fisher criterion, achieving optimal separability in terms of spatial and distances distribution (cf. Table 1). (*Label Propagation*, bottom right) The structural analysis is exploited to classify previously unseen responses generated under the same setting: here, separability in the embedding space is potentially scarce, requiring the usage of Fisher space for reliable performances (cf. Table 2): points are classified by the distributions of the point-to-clusters distances.

3. Methodology

We now describe the framework used to analyse response variability and hallucination behaviour. Our approach is organised around three complementary components. First, we describe how the dataset is generated (see also Section A). Second, we perform a structural analysis of embedded responses to characterise geometric and distributional differences between genuine and hallucinated outputs. Third, we leverage this structure to define a supervised label-propagation scheme that extends small sets of annotated responses to larger collections without additional supervision.

3.1. Dataset

Our analysis focuses on factual hallucinations, where responses contain false or misleading information presented as facts (Sun et al., 2024). We adopt time-sensitive questions to assess the trustworthiness of LLMs on evolving factual queries (Zhu et al., 2025). This choice is motivated by empirical evidence that smaller models exhibit substantially weaker performance on time-sensitive questions, making them more susceptible to hallucination about temporal events (Pezik et al., 2025). Furthermore, these models show increased reliability with repeated sampling (Brown et al., 2024), but existing analyses do not provide a quantitative metric for hallucination rates.

We employ 10 small-sized (up to 32B) LLMs with publicly available weights,¹ selected to represent a range of

¹Namely: deepseek-llm-7b-base, Mistral-7B-v0.1, Llama-3.1-8B, Yi-1.5-9B, Gemma-2-9b, SOLAR-10.7B-v1.0, Phi-4, Qwen2.5-14B, Gemma-2-27b, and Qwen2.5-32B.

model families, architectural variations, and parameter scales, while maintaining comparability in size. Crucially, all models are base variants, i.e., pretrained models without instruction or alignment fine-tuning, ensuring that observed behaviours reflect fundamental generation properties rather than task-specific conditioning.

We crafted our prompts to target precise information about 100 repetitive events occurring in 2020 and 2022, allowing us to analyze how factual knowledge stability evolves (Zhu et al., 2025) within a controlled setting where both years fall demonstrably within the training boundaries of all evaluated models (Pezik et al., 2025). For each model-prompt pair, we generate 150 independent responses under identical sampling conditions, yielding a total of 300,000 responses, *i.e.*

$$\underbrace{100}_{\text{prompts}} \times \underbrace{2}_{\text{years}} \times \underbrace{150}_{\text{responses}} \times \underbrace{10}_{\text{models}} = 300,000, \text{ of which}$$

231,473 (77.16%) remain after filtering for class imbalance and annotation uncertainty (cf. Table 4). To study the impact of representation on geometric structure, we analyse each response under two embedding regimes: (i) complete responses, embedded directly using the sentence encoder; and (ii) stemmed responses, obtained by applying morphological stemming to reduce lexical variation while preserving semantic content. In what follows, we focus on complete responses, while results related to stemmed responses can be found in Appendix C.1.

LLM-as-a-Judge Evaluation We adopt an LLM-as-a-judge strategy to categorize model responses as *genuine* (G, factually correct), *hallucinated* (H), or *unknown* (U), where the latter corresponds to responses that explicitly acknowledge uncertainty or lack of knowledge. Large-sized

LLM judging has recently emerged as a scalable alternative to human annotation for assessing factual correctness, reasoning quality, and independent evaluation of model outputs (Zheng et al., 2023; Pezik et al., 2025), demonstrating strong correlation with human judgments at a fraction of the cost (Liu et al., 2023). We employ this paradigm using a fixed, high-capacity, proprietary model (Claude 4.5 Sonnet), treated here as an external oracle. Responses labeled as *unknown* are excluded from the present analysis, allowing us to focus on the geometric and statistical properties of factually grounded versus hallucinated generations. This labeling step transforms unstructured collections of stochastic model outputs into labeled sets in embedding space. The annotation enables the study of distributional structure, separability, and failure behavior, also supporting the propagation of annotations from a limited number of judged responses to larger sets of generated responses.

To assess the reliability of the automatically assigned labels, we conducted a manual validation. A total of 1,000 instances ($\approx 0.4\%$ of the full dataset) were independently annotated by two computer science PhD students. Of these, 800 instances were annotated separately (i.e., 400 per annotator), while 200 instances were annotated by both. On the shared subset, the annotators agreed on 94% of the cases (Cohen’s $\kappa = 0.86$), indicating strong agreement. Disagreements were adjudicated by a senior researcher acting as an independent super-annotator. Comparing the finalized human annotations against Claude’s labels on the full set of 1,000 instances shows that Claude’s annotations match the human consensus in 87.90% of the cases, supporting the accuracy and suitability of Claude-generated labels.

3.2. Notation and Setting

In what follows, let q denote a fixed prompt and let $\mathcal{R} = \{r_1, \dots, r_N\}$ be a set of N responses generated independently by an LLM under identical decoding conditions. Each response is embedded using the fixed sentence encoder ϕ , yielding vectors $\mathbf{x}_i \in \mathbb{R}^{384}$.

A subset $\mathcal{R}_t \subseteq \mathcal{R}$ of size $N_t \leq N$ is assigned semantic correctness labels $y_i \in \{G, H\}$, corresponding to genuine and hallucinated responses, respectively. We denote by \mathcal{X}_G and \mathcal{X}_H the sets of embedded responses corresponding to genuine and hallucinated outputs from \mathcal{R}_t .

3.3. Structural Analysis of Response Geometry

Our analysis is motivated by the empirical hypothesis that, for a given prompt, genuine responses exhibit greater semantic consistency than hallucinated responses. Informally, correct answers tend to concentrate around a stable semantic core, while hallucinations manifest greater variability, reflecting distinct fabricated or erroneous explanations. This suggests that genuine and hallucinated responses should

exhibit different geometric signatures in embedding space.

To test this assumption, we analyse pairwise distances within and across labelled responses. Given two embedded responses $\mathbf{x}_i, \mathbf{x}_j$, we compute the Euclidean distance $\|\mathbf{x}_i - \mathbf{x}_j\|_2$. From these distances, we derive three empirical distributions: (i) intra-genuine distances \mathcal{D}_{GG} , (ii) intra-hallucinated distances \mathcal{D}_{HH} , and (iii) inter-class distances \mathcal{D}_{GH} .

Rather than summarising these distributions through low-order moments, we compare them using the one-dimensional Wasserstein distance. Specifically, we quantify separation by measuring the Wasserstein distance between \mathcal{D}_{GG} and \mathcal{D}_{HH} and comparing it to the same distance evaluated on the null hypothesis H_0 obtained by randomly permuting class labels. This allows us to assess both the statistical significance of observed differences and their deviation from chance-level structure.

To complement the distributional analysis, we assess linear separability between genuine and hallucinated responses using Fisher Discriminant Analysis (FDA).² Given the labeled embeddings $\mathcal{X}_G \cup \mathcal{X}_H$, we compute class means μ_G and μ_H , and the within-class scatter matrix

$$\mathbf{S}_W = \sum_{\mathbf{x} \in \mathcal{X}_G} (\mathbf{x} - \mu_G)(\mathbf{x} - \mu_G)^\top + \sum_{\mathbf{x} \in \mathcal{X}_H} (\mathbf{x} - \mu_H)(\mathbf{x} - \mu_H)^\top.$$

To ensure numerical stability in high-dimensional settings, we adopt the regularised formulation $\mathbf{S}_W^{(\lambda)} = \mathbf{S}_W + \lambda \mathbf{I}_d$, where $\lambda > 0$ controls the strength of regularisation. The Fisher discriminant direction is then given, up to scale, by $\mathbf{v} \propto \left(\mathbf{S}_W^{(\lambda)}\right)^{-1} (\mu_G - \mu_H)$. Projection onto \mathbf{v} yields a one-dimensional representation in which genuine and hallucinated responses can be directly compared, and mutual distances are moved from \mathcal{D}_{GG} (\mathcal{D}_{HH} , \mathcal{D}_{GH}) to Δ_{GG} (Δ_{HH} , Δ_{GH}). This step serves as a diagnostic tool, revealing whether the two response types occupy distinct regions of embedding space under linear projections.

3.4. Supervised Label Propagation

Building on the structural properties revealed by the previous analysis, we define a supervised procedure to propagate labels from a small annotated subset \mathcal{R}_t to the remaining responses in $\mathcal{R} \setminus \mathcal{R}_t$.

Using the Fisher direction \mathbf{v} estimated from \mathcal{R}_t , each embedded response $\mathbf{x} \in \mathbb{R}^d$ is mapped to a scalar coordinate: $z = \mathbf{v}^\top \mathbf{x}$. This projection induces a one-dimensional representation in which distances reflect discriminative variation between genuine and hallucinated responses.

For a given unlabelled response r with projection z , we

²Appendix D presents a comparison between FDA and other non-linear projection methods.

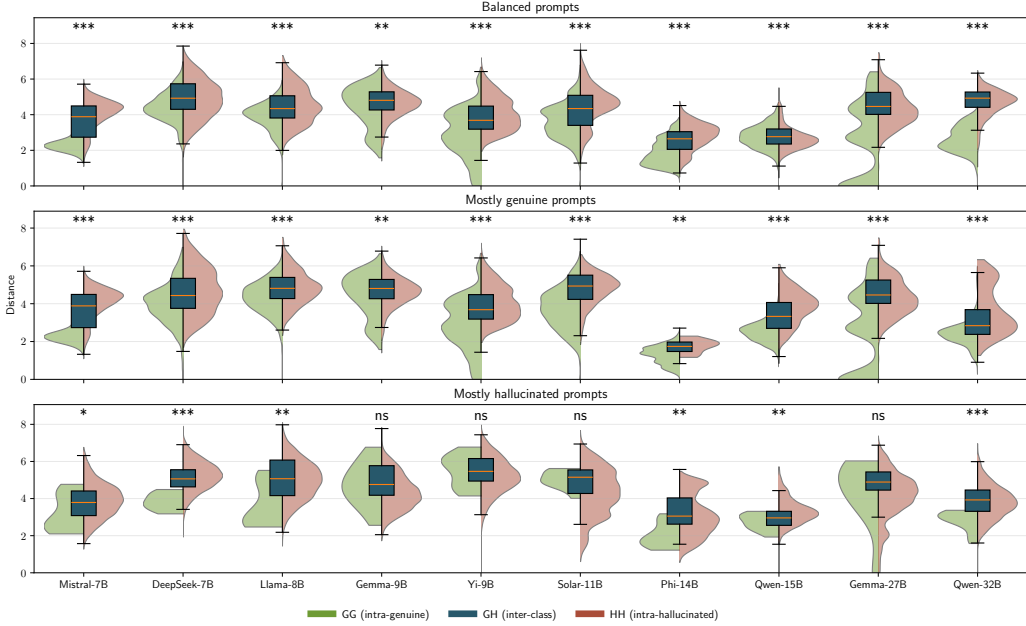


Figure 2. Distributions of mutual intra-class distances for Genuine (\mathcal{D}_{GG} , green) and Hallucinated (\mathcal{D}_{HH} , red) responses. Inter-class distance distributions \mathcal{D}_{GH} are overlaid as blue boxplots, with medians highlighted. Statistical significance, assessed using Wilcoxon test, refers to differences between \mathcal{D}_{GG} and \mathcal{D}_{HH} : *** $p < .001$, ** $p < .01$, * $p < .05$, ns otherwise.

compute the distances to the projected points of each labelled class, yielding the point-to-set distance collections: $\Delta_G(z) = \{ |z - z_i| : z_i \in \mathcal{Z}_G \}$ and $\Delta_H(z) = \{ |z - z_i| : z_i \in \mathcal{Z}_H \}$, where \mathcal{Z}_G and \mathcal{Z}_H denote the projection of \mathcal{X}_G and \mathcal{X}_H .

These collections define empirical distance distributions, which, consistently with the structural analysis above, are compared to the corresponding intra-class distance distributions using the Wasserstein distance. Intuitively, a response is assigned to the class for which its induced distance distribution is more consistent with the internal structure of that class. In other words, we assign r to the class minimising the Wasserstein discrepancy between $\Delta_r(z)$ and the reference intra-class distribution Δ_{∞} , or, in formulas, the response is classified as Hallucinated if $W(\Delta_{GG}, \Delta_r) > W(\Delta_{HH}, \Delta_r)$.

While this procedure resembles classical linear discriminant classification under Euclidean distance, its formulation in terms of distributional consistency aligns naturally with the structural analysis developed earlier. This perspective allows classification decisions to be interpreted geometrically, in terms of conformity with the observed internal organisation of response clusters, rather than solely in terms of pointwise distance to a decision boundary.

4. Results

We now present the empirical results obtained by applying the proposed framework to the responses generated by the considered set of small-sized language models.

4.1. Structural analysis of responses

Figure 2 reports the empirical distributions of pairwise distances within and across response classes, computed in the sentence embedding space. For each model–prompt pair, we consider three distributions: intra-genuine distances \mathcal{D}_{GG} , intra-hallucinated distances \mathcal{D}_{HH} , and inter-class distances \mathcal{D}_{GH} . The comparison between \mathcal{D}_{GG} and \mathcal{D}_{HH} is statistically assessed using a Wilcoxon rank-sum test, whose outcome is reported above each panel.

Across all models, we observe a consistent structural asymmetry between genuine and hallucinated responses. In particular, intra-genuine distances tend to be smaller than inter-class distances, indicating that factually correct answers exhibit higher semantic cohesion. This difference is statistically significant in the large majority of cases, often at the $p < 10^{-3}$ level. However, despite this consistency, the distributions remain substantially overlapping: the inter-class distances (blue boxplots) are often entangled with both \mathcal{D}_{GG} and \mathcal{D}_{HH} , especially in the presence of class imbalance. This highlights an important limitation of directly exploiting pairwise distances in the original embedding space: although a structural signal exists, it is not readily separable without additional information.

The robustness of this structural signal is further illustrated by the comparison against a null hypothesis H_0 . Figure 3 shows a representative example for qwen2.5-32B, where prompts are ordered according to the observed Wasserstein

Table 1. Mean (std) of the ratio between intra- and inter-class distances.

Model	Original space	Fisher space
mistral-7B	1.09 (0.08)	7.45 (5.68)
deepseek-7B	1.12 (0.10)	9.44 (5.71)
llama3-8B	1.11 (0.09)	7.71 (5.23)
gemma2-9B	1.08 (0.07)	6.51 (4.25)
yi1.5-9B	1.21 (0.13)	9.53 (6.21)
solar1-11B	1.09 (0.07)	5.29 (5.73)
phi4-14B	<u>1.19 (0.21)</u>	5.82 (4.96)
qwen2.5-14B	1.15 (0.11)	6.16 (6.50)
gemma2-27B	1.11 (0.11)	7.46 (4.24)
qwen2.5-32B	1.17 (0.15)	7.25 (7.46)
Average	1.13 (0.11)	7.26 (5.60)

distance between \mathcal{D}_{GG} and \mathcal{D}_{HH} . For each prompt, the observed distance is compared with the distribution obtained under H_0 , constructed by randomly permuting class labels. For the vast majority of prompts, the observed Wasserstein distance exceeds the null expectation by a substantial margin, often by multiple factors. This confirms that the separation between genuine and hallucinated responses is not an artefact of sample size or marginal distributions, but reflects a genuine geometric difference in embedding space. A complete quantitative summary across models and prompts is provided in Appendix C.

While statistically robust, this separation remains difficult to exploit directly. To make the structural difference operational, we project the responses onto the one-dimensional subspace identified by the FDA, evaluated with $\lambda = 1.2$ (see later Figure 5). Table 1 quantifies the resulting gain in separability by reporting the ratio between inter-class and intra-class distances, computed both in the original embedding space and after Fisher projection. In the regular space, the ratio $2\mathcal{D}_{GH}/(\mathcal{D}_{GG} + \mathcal{D}_{HH})$ remains close to one for all models, indicating that inter- and intra-class distances are of comparable magnitude. After projection, separability increases consistently across all considered models, with an average amplification factor $2\Delta_{GH}/(\Delta_{GG} + \Delta_{HH})$ of $7.26 \times$.

This result shows that FDA effectively concentrates the structural signal identified by the Wasserstein analysis into a single discriminative direction. The combination of distributional evidence and linear separability suggests that genuine and hallucinated responses occupy distinct, though initially entangled, regions of semantic space. This observation directly motivates the supervised propagation strategy introduced in the following section, where the Fisher projection is used to extend reliable labels from a small tagged subset to a larger pool of unlabelled responses.

4.2. Label propagation

The structural analysis presented above establishes the existence of a consistent geometric distinction between genuine and hallucinated responses. Rather than attempting global

Table 2. Mean (std) of the label propagator performances.

Model	Accuracy	F1	Signed Margin		Absolute Margin	
			G	H	G	H
mistral-7B	86.8 (6.6)	92.1 (4.4)	-0.1 (0.3)	-0.6 (0.3)	0.4 (0.2)	0.7 (0.2)
deepseek-7B	90.9 (6.2)	94.1 (4.8)	0.4 (0.5)	-1.1 (0.5)	0.8 (0.3)	1.2 (0.4)
llama3-8B	89.1 (6.3)	92.5 (5.7)	0.3 (0.5)	-0.9 (0.5)	0.7 (0.3)	1.0 (0.3)
gemma2-9B	86.1 (7.1)	91.5 (5.0)	-0.0 (0.4)	-0.7 (0.4)	0.5 (0.2)	0.7 (0.3)
yi1.5-9B	92.5 (4.8)	95.3 (3.7)	0.5 (0.5)	-1.1 (0.5)	0.9 (0.3)	1.1 (0.3)
solar1-11B	82.7 (9.1)	86.9 (8.2)	0.2 (0.3)	-0.5 (0.4)	0.5 (0.2)	0.6 (0.2)
phi4-14B	85.2 (9.6)	84.0 (16.8)	0.3 (0.2)	-0.4 (0.3)	0.4 (0.1)	0.5 (0.2)
qwen2.5-14B	85.0 (8.8)	88.7 (9.1)	0.2 (0.3)	-0.5 (0.3)	0.4 (0.2)	0.6 (0.2)
gemma2-27B	88.3 (6.9)	93.0 (4.5)	-0.0 (0.4)	-0.8 (0.4)	0.6 (0.2)	0.8 (0.3)
qwen2.5-32B	85.5 (8.7)	89.1 (9.0)	0.2 (0.3)	-0.6 (0.3)	0.4 (0.2)	0.6 (0.2)
Average	87.2 (7.4)	90.7 (7.1)	0.2 (0.4)	-0.7 (0.4)	0.6 (0.2)	0.8 (0.3)

transfer, we exploit this structure locally by framing label inference as a *prompt- and model-conditioned propagation problem*, where a small set of validated responses is used to infer the labels of the remaining ones.

Table 2 summarises the performance of the proposed label propagator across all models. For each prompt and model, we consider the full set of generated responses and perform 20 stratified splits into training and test sets, with a 2/3-1/3 ratio while preserving the proportion of genuine and hallucinated responses. All reported metrics are averaged over prompts and splits.

Across models, the propagator achieves strong and stable performance, with an average accuracy of 87.2% and F1-score of 90.7%. Performance varies moderately across architectures, ranging from 82.7% accuracy for `solar1-11B` to 92.5% for `yi1.5-9B`, but remains consistently high for all considered models. Moreover, our performances do not scale monotonically with model size: smaller models such as `yi1.5-9B` and `deepseek-7B` outperform substantially larger ones, reinforcing the observation that separability is independent of parameter size.

Beyond classification accuracy, Table 2 reports both signed and absolute margins, defined as $W(\Delta_{HH}, \Delta_H) - W(\Delta_{GG}, \Delta_G)$, which quantify how decisively a response is assigned to a class. Signed margins reveal a systematic asymmetry: hallucinated responses tend to be classified with larger magnitude margins than genuine ones, indicating that they are more clearly separated from the genuine cluster in Fisher space. Absolute margins, instead, measure confidence independently of direction and show consistent separation across both classes. Together, these results suggest that the propagator is not only accurate, but also internally consistent in how it evaluates proximity to class structure.

A key motivation for label propagation is to reduce the reliance on costly annotations. Figure 4 investigates how performance evolves as a function of the number of labelled responses. Here, test sets are fixed to one third of the available responses, while the training set size is increased from 5 to 100 in steps of 5. Along with the multiple stratified

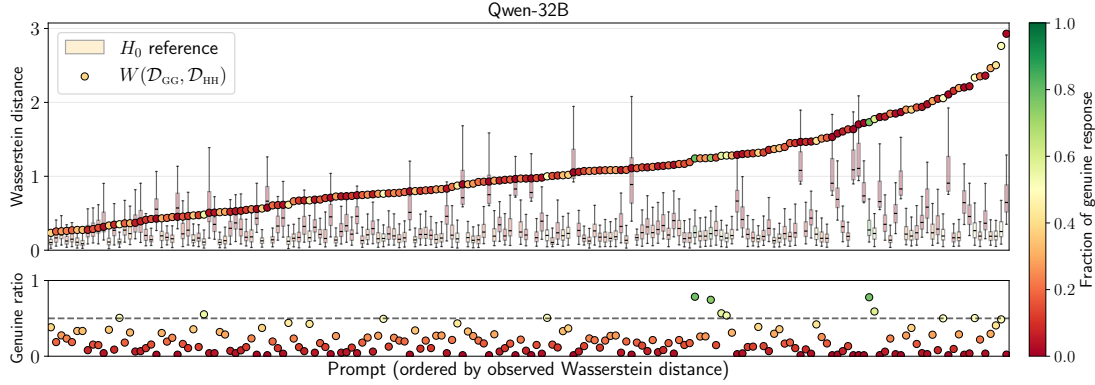


Figure 3. Statistical relevance of the distributional separation between \mathcal{D}_{GG} and \mathcal{D}_{HH} over the various prompts for qwen2.5-32B. (Top) The observed Wasserstein distance $W(\mathcal{D}_{\text{GG}}, \mathcal{D}_{\text{HH}})$, represented by ordered dots, is compared with the same distance evaluated on the null hypothesis H_0 obtained permuting labels 100 times. (Bottom) Fraction of genuine responses is reported for each prompt, also encoded in the color channel.

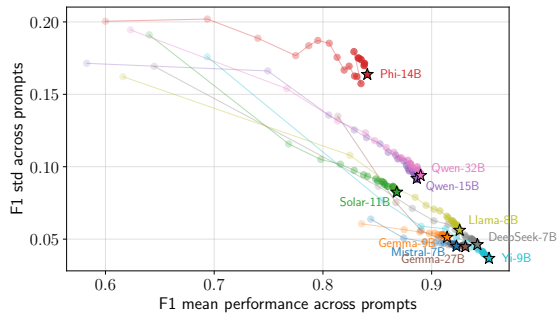


Figure 4. Evolution of the label propagator F1-score with the increase of the training set size from 5 to 100 responses (step 5). Results are in terms of mean (x-axis) and standard deviation (y-axis): the lower and righter, the better (cf. Figure 8).

splits, when the training size does not exhaust the available data, results are averaged over 10 random subsamplings, using the same underlying train–test splits.

Across all models, performance improves rapidly with the number of labelled examples and then saturates. In particular, both accuracy and F1-score exhibit diminishing returns beyond approximately 30 labelled responses, with near-saturation reached around 50–60 samples. At the same time, variability across splits decreases monotonically as the training set grows. This behaviour is remarkably consistent across architectures, with the only notable exception being phi 4–14B, whose improvement remains more gradual. These results indicate that the propagator can operate effectively in low-supervision regimes, requiring a small set of validated responses to achieve strong performance.

Finally, Figure 5 analyses the sensitivity of the propagator to the regularisation parameter λ used in the Fisher evaluation. Despite evaluating λ over several orders of magnitude, performance exhibits a sharply defined optimum that is shared

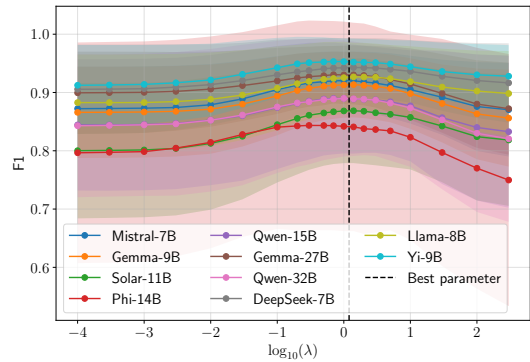


Figure 5. Sensitivity analysis of the λ regularisation parameter for each of the models. Best choice is reported as a dashed black line.

across all models. Strikingly, a single value ($\lambda \approx 1.2$) maximises performance, minimising the regret for every architecture considered.

5. Discussion

Our results support a geometric and structural interpretation of LLM-generated hallucinated responses that departs from the common framing of hallucination as a mere failure of knowledge or memorisation. Instead, the evidence points toward systematic properties of how language models retrieve, organise, and project information in semantic space.

Insight 1: *Hallucinations are not primarily caused by lack of knowledge, but by failures in information retrieval.*

Across all evaluated models, the same prompt can yield both correct and hallucinated responses under repeated sampling. This observation, already noted anecdotally in prior work, acquires here a structural interpretation: the knowledge required to answer is present in the model, yet retrieval

“occasionally” deviates toward semantically plausible but factually inconsistent regions. This reframes hallucination as a process-level failure rather than a static absence of information, with implications for mitigation strategies that move their focus on decoding, conditioning, or retrieval guidance rather than parameter scaling alone.

Insight 2: *Hallucinated responses exhibit a consistent geometric signature in embedding space, characterised by reduced semantic cohesion relative to genuine answers.*

Distance-based analyses reveal that hallucinated responses systematically display weaker internal cohesion and altered inter-class relationships when compared to genuine ones. This effect is stable across models of different sizes and architectures, across prompts, and under varying class balances. Crucially, permutation-based controls and null comparisons prompt that the observed separability is not a by-product of marginal distributions, sample size, or label imbalance. Hallucination thus emerges as a geometric phenomenon, detectable at the level of response distributions rather than at the level of individual points.

Insight 3: *Hallucination-related variance concentrates along a low-dimensional direction in (semantical) embedding space.*

While separability in the original embedding space remains limited, FDA consistently identifies a single direction along which the distinction between genuine and hallucinated responses becomes pronounced. This suggests that factual inconsistency manifests coherently, aligning along a low-dimensional semantic axis rather than being diffusely distributed. The effectiveness of this projection supports the hypothesis that hallucinations can be interpreted as structured displacements within the embedding manifold.

Insight 4: *Structural regularities enable label-efficient classification through geometry-aware propagation.*

Once the relevant structure is exposed, supervision becomes remarkably cheap. Using as few as 30–60 labelled responses, the proposed propagation strategy achieves stable and competitive performance across all evaluated models. Importantly, performance does not scale with model size, reinforcing the view that the driving factor is geometric organisation rather than architectural complexity.

Insight 5: *A single Fisher regularisation scale generalises across models, suggesting embedding-induced universality.*

The emergence of a shared optimal regularisation value ($\lambda \approx 1.2$) across all models is surprising given their architectural diversity. This points to a common geometric scale induced by the embedding space itself, where responses generated by different models are mapped coherently. Beyond

simplifying deployment, this property indicates that embedding quality plays a central role in hallucination detectability, and that model-specific tuning might be unnecessary.

Beyond these central insights, our results confirm a well-known but still practically relevant limitation: small-sized LLMs remain particularly inefficient at retrieving correct factual and temporal information. While not novel per se, this observation contextualises the stronger geometric instability observed for such models and reinforces the importance of retrieval-aware analysis when comparing architectures of different capacities.

Limitations and future directions The present study focuses on prompt-local structural analysis and does not explore the coherence of discriminative directions across prompts or tasks. While this choice allows for controlled and interpretable comparisons, it does not address the extent to which discriminative directions or geometric signatures align across different prompts, domains, or tasks. Understanding whether Fisher projections exhibit coherence or transferability across prompts and models represents an important next step, with potential implications for global detection strategies and prompt-agnostic reliability measures.

More broadly, our analysis is grounded in a specific embedding choice and in factual, time-sensitive queries, which offer a convenient testbed but capture only a subset of hallucination phenomena. Extending this framework to other embedding spaces, response types, and hallucination categories would help clarify which observed geometric regularities are intrinsic to hallucination itself and which depend on representational or task-specific factors. Finally, while label efficiency and regularisation stability suggest a degree of robustness, further work is needed to assess how these properties interact with alternative judging protocols, prompt conditioning strategies, and multi-prompt aggregation schemes.

6. Conclusion

We have shown that hallucinations in small-sized LLMs are strongly linked to structural patterns in the embedding space rather than purely to missing knowledge. Indeed, genuine responses exhibit higher semantic cohesion, while hallucinated ones form distinct distributions, with inter- versus intra-class distance ratios increasing on average from 1.13 in the original embedding space to 7.26 along the Fisher discriminant direction. Leveraging the above introduced result, we built a label-propagation framework that achieves F1 scores above 90% across all models.

These results suggest that the embedding-space geometry provides both a diagnostic and a practical tool for scalable hallucination detection, complementing existing knowledge-centric or single-response evaluation paradigms.

Impact Statement

This work contributes to the understanding of hallucinations in small-sized language models by framing them through a geometrical interpretation in the embedding space rather than solely as a consequence of missing knowledge. This framework also enable the label-efficient propagation of hallucinated responses under repeated sampling. A direct application of this finding could also support more reliable evaluation and monitoring of language models in practical settings, particularly where small or open-weight models are deployed.

Potential positive impacts include improved trustworthiness assessment, better benchmarking of stochastic model behaviour, and reduced annotation costs for hallucination analysis. The proposed methodology is diagnostic rather than generative: it does not modify model outputs or increase the likelihood of harmful content generation.

The primary risks are indirect and limited to misuse for overconfident filtering. We mitigate this by positioning our method as an analytical and evaluation tool, intended to complement –not replace– existing factuality checks and human judgement.

References

Bang, Y., Ji, Z., Schelten, A., Hartshorn, A., Fowler, T., Zhang, C., Cancedda, N., and Fung, P. HalluLens: LLM hallucination benchmark. In Che, W., Nabende, J., Shutova, E., and Pilehvar, M. T. (eds.), *Proceedings of the 63rd Annual Meeting of the Association for Computational Linguistics (Volume 1: Long Papers)*, pp. 24128–24156, Vienna, Austria, July 2025. Association for Computational Linguistics. ISBN 979-8-89176-251-0. doi: 10.18653/v1/2025.acl-long.1176. URL <https://aclanthology.org/2025.acl-long.1176/>.

Bar-Shalom, G., Frasca, F., Galron, Y., Ziser, Y., and Maron, H. Beyond token probes: Hallucination detection via activation tensors with act-vit. *arXiv preprint arXiv:2510.00296*, 2025.

Bayat, F. F., Zhang, L., Munir, S., and Wang, L. Factbench: A dynamic benchmark for in-the-wild language model factuality evaluation. In *Proceedings of the 63rd Annual Meeting of the Association for Computational Linguistics (Volume 1: Long Papers)*, pp. 33090–33110, 2025.

Belcak, P., Heinrich, G., Diao, S., Fu, Y., Dong, X., Muralidharan, S., Lin, Y. C., and Molchanov, P. Small language models are the future of agentic ai. *arXiv preprint arXiv:2506.02153*, 2025.

Bender, E. M., Gebru, T., McMillan-Major, A., and Shmitchell, S. On the dangers of stochastic parrots: Can language models be too big? In *Proceedings of the 2021 ACM Conference on Fairness, Accountability, and Transparency*, FAccT '21, pp. 610–623. ACM, March 2021. doi: 10.1145/3442188.3445922. URL <http://dx.doi.org/10.1145/3442188.3445922>.

Brown, B., Juravsky, J., Ehrlich, R., Clark, R., Le, Q. V., Ré, C., and Mirhoseini, A. Large language monkeys: Scaling inference compute with repeated sampling, 2024. URL <https://arxiv.org/abs/2407.21787>.

Chafekar, T., Goindani, A., Liang, P. P., Mathur, L., Morency, L.-P., Salakhutdinov, R., and Yu, H. Hemm: Holistic evaluation of multimodal foundation models. In *Advances in Neural Information Processing Systems 37*, NeurIPS 2024, pp. 42899–42940. Neural Information Processing Systems Foundation, Inc. (NeurIPS), 2024. doi: 10.52202/079017-1358. URL <http://dx.doi.org/10.52202/079017-1358>.

Chung, H. W., Hou, L., Longpre, S., Zoph, B., Tay, Y., Fedus, W., Li, Y., Wang, X., Dehghani, M., Brahma, S., et al. Scaling instruction-finetuned language models. *Journal of Machine Learning Research*, 25(70):1–53, 2024.

Farquhar, S., Kossen, J., Kuhn, L., and Gal, Y. Detecting hallucinations in large language models using semantic entropy. *Nature*, 630(8017):625–630, 2024.

Fisher, R. A. The use of multiple measurements in taxonomic problems. *Annals of Eugenics*, 7(2):179–188, September 1936. ISSN 2050-1439. doi: 10.1111/j.1469-1809.1936.tb02137.x. URL <http://dx.doi.org/10.1111/j.1469-1809.1936.tb02137.x>.

Han, J., Kossen, J., Razzak, M., and Gal, Y. Semantic entropy neurons: Encoding semantic uncertainty in the latent space of llms. In *MINT: Foundation Model Interventions*, 2024. URL [https://openreview.net/forum?id=BbZKxrZCNn&referrer=%5Bthe%20profile%20of%20Yarin%20Gal%5D\(%2Fprofile%3Fid%3D~Yarin_Gall1\)](https://openreview.net/forum?id=BbZKxrZCNn&referrer=%5Bthe%20profile%20of%20Yarin%20Gal%5D(%2Fprofile%3Fid%3D~Yarin_Gall1)).

Hao, G., Wu, J., Pan, Q., and Morello, R. Quantifying the uncertainty of llm hallucination spreading in complex adaptive social networks. *Scientific reports*, 14(1):16375, 2024.

Huang, L., Yu, W., Ma, W., Zhong, W., Feng, Z., Wang, H., Chen, Q., Peng, W., Feng, X., Qin, B., et al. A survey on hallucination in large language models: Principles, taxonomy, challenges, and open questions. *ACM Transactions on Information Systems*, 2023.

Huang, Y., Sun, L., Wang, H., Wu, S., Zhang, Q., Li, Y., Gao, C., Huang, Y., Lyu, W., Zhang, Y., Li, X., Sun, H., Liu,

Z., Liu, Y., Wang, Y., Zhang, Z., Vidgen, B., Kailkhura, B., Xiong, C., Xiao, C., Li, C., Xing, E. P., Huang, F., Liu, H., Ji, H., Wang, H., Zhang, H., Yao, H., Kellis, M., Zitnik, M., Jiang, M., Bansal, M., Zou, J., Pei, J., Liu, J., Gao, J., Han, J., Zhao, J., Tang, J., Wang, J., Vanschoren, J., Mitchell, J., Shu, K., Xu, K., Chang, K.-W., He, L., Huang, L., Backes, M., Gong, N. Z., Yu, P. S., Chen, P.-Y., Gu, Q., Xu, R., Ying, R., Ji, S., Jana, S., Chen, T., Liu, T., Zhou, T., Wang, W. Y., Li, X., Zhang, X., Wang, X., Xie, X., Chen, X., Wang, X., Liu, Y., Ye, Y., Cao, Y., Chen, Y., and Zhao, Y. Trustllm: Trustworthiness in large language models. In *Forty-first International Conference on Machine Learning*, 2024. URL <https://openreview.net/forum?id=bWUU0LwwMp>.

Jacovi, A., Wang, A., Alberti, C., Tao, C., Lipovetz, J., Oliszewska, K., Haas, L., Liu, M., Keating, N., Bloniarz, A., et al. The facts grounding leaderboard: Benchmarking llms' ability to ground responses to long-form input. *arXiv preprint arXiv:2501.03200*, 2025.

Ji, Z., Lee, N., Frieske, R., Yu, T., Su, D., Xu, Y., Ishii, E., Bang, Y. J., Madotto, A., and Fung, P. Survey of hallucination in natural language generation. *ACM computing surveys*, 55(12):1–38, 2023.

Jiang, L., Chai, Y., Li, M., Liu, M., Fok, R., Dziri, N., Tsvetkov, Y., Sap, M., Albalak, A., and Choi, Y. Artificial hivemind: The open-ended homogeneity of language models (and beyond). *arXiv preprint arXiv:2510.22954*, 2025.

Kalai, A. T., Nachum, O., Vempala, S. S., and Zhang, E. Why language models hallucinate. *arXiv preprint arXiv:2509.04664*, 2025.

Kuhn, L., Gal, Y., and Farquhar, S. Semantic uncertainty: Linguistic invariances for uncertainty estimation in natural language generation. In *NeurIPS ML Safety Workshop*, 2022. URL https://openreview.net/forum?id=tWS-S_aRDRe.

Li, J., Cheng, X., Zhao, W. X., Nie, J.-Y., and Wen, J.-R. Halueval: A large-scale hallucination evaluation benchmark for large language models. In *Proceedings of the 2023 Conference on Empirical Methods in Natural Language Processing*, pp. 6449–6464, 2023.

Lin, S., Hilton, J., and Evans, O. Truthfulqa: Measuring how models mimic human falsehoods. In *Proceedings of the 60th Annual Meeting of the Association for Computational Linguistics (Volume 1: Long Papers)*, 2022.

Ling, C., Zhao, X., Zhang, X., Cheng, W., Liu, Y., Sun, Y., Oishi, M., Osaki, T., Matsuda, K., Ji, J., Bai, G., Zhao, L., and Chen, H. Uncertainty quantification for in-context learning of large language models. In Duh, K., Gomez, H., and Bethard, S. (eds.), *Proceedings of the 2024 Conference of the North American Chapter of the Association for Computational Linguistics: Human Language Technologies (Volume 1: Long Papers)*, pp. 3357–3370, Mexico City, Mexico, June 2024. Association for Computational Linguistics. doi: 10.18653/v1/2024.nacl-long.184. URL [https://aclanthology.org/2024.nacl-long.184/](https://aclanthology.org/2024.nacl-long.184).

Liu, Y., Iter, D., Xu, Y., Wang, S., Xu, R., and Zhu, C. G-eval: NLG evaluation using gpt-4 with better human alignment. In Bouamor, H., Pino, J., and Bali, K. (eds.), *Proceedings of the 2023 Conference on Empirical Methods in Natural Language Processing*, pp. 2511–2522, Singapore, December 2023. Association for Computational Linguistics. doi: 10.18653/v1/2023.emnlp-main.153. URL [https://aclanthology.org/2023.emnlp-main.153/](https://aclanthology.org/2023.emnlp-main.153).

Manakul, P., Liusie, A., and Gales, M. SelfCheckGPT: Zero-resource black-box hallucination detection for generative large language models. In Bouamor, H., Pino, J., and Bali, K. (eds.), *Proceedings of the 2023 Conference on Empirical Methods in Natural Language Processing*, pp. 9004–9017, Singapore, December 2023. Association for Computational Linguistics. doi: 10.18653/v1/2023.emnlp-main.557. URL [https://aclanthology.org/2023.emnlp-main.557/](https://aclanthology.org/2023.emnlp-main.557).

Min, S., Krishna, K., Lyu, X., Lewis, M., Yih, W.-t., Koh, P., Iyyer, M., Zettlemoyer, L., and Hajishirzi, H. FActScore: Fine-grained atomic evaluation of factual precision in long form text generation. In Bouamor, H., Pino, J., and Bali, K. (eds.), *Proceedings of the 2023 Conference on Empirical Methods in Natural Language Processing*, pp. 12076–12100, Singapore, December 2023. Association for Computational Linguistics. doi: 10.18653/v1/2023.emnlp-main.741. URL [https://aclanthology.org/2023.emnlp-main.741/](https://aclanthology.org/2023.emnlp-main.741).

Niu, M., Haddadi, H., and Pang, G. Robust hallucination detection in llms via adaptive token selection. *arXiv preprint arXiv:2504.07863*, 2025.

Ouyang, L., Wu, J., Jiang, X., Almeida, D., Wainwright, C., Mishkin, P., Zhang, C., Agarwal, S., Slama, K., Ray, A., Schulman, J., Hilton, J., Kelton, F., Miller, L., Simens, M., Askell, A., Welinder, P., Christiano, P. F., Leike, J., and Lowe, R. Training language models to follow instructions with human feedback. In Koyejo, S., Mohamed, S., Agarwal, A., Belgrave, D., Cho, K., and Oh, A. (eds.), *Advances in Neural Information Processing Systems*, volume 35, pp. 27730–27744. Curran Associates, Inc., 2022.

Pezik, P., Kaczynski, K., Szymanska, M., Zarnecki, F., Deckert, Z., Kwiatkowski, J., and Janowski, W. Llm-lagbench: Identifying temporal training boundaries in

large language models. *arXiv preprint arXiv:2511.12116*, 2025.

Qi, X., Panda, A., Lyu, K., Ma, X., Roy, S., Beirami, A., Mittal, P., and Henderson, P. Safety alignment should be made more than just a few tokens deep. In Yue, Y., Garg, A., Peng, N., Sha, F., and Yu, R. (eds.), *International Conference on Representation Learning*, volume 2025, pp. 54911–54941, 2025.

Reimers, N. and Gurevych, I. Sentence-BERT: Sentence embeddings using Siamese BERT-networks. In Inui, K., Jiang, J., Ng, V., and Wan, X. (eds.), *Proceedings of the 2019 Conference on Empirical Methods in Natural Language Processing and the 9th International Joint Conference on Natural Language Processing (EMNLP-IJCNLP)*, pp. 3982–3992, Hong Kong, China, November 2019. Association for Computational Linguistics. doi: 10.18653/v1/D19-1410. URL <https://aclanthology.org/D19-1410/>.

Sriramanan, G., Bharti, S., Sadasivan, V. S., Saha, S., Katalkinda, P., and Feizi, S. Llm-check: Investigating detection of hallucinations in large language models. *Advances in Neural Information Processing Systems*, 37: 34188–34216, 2024.

Su, W., Wang, C., Ai, Q., Hu, Y., Wu, Z., Zhou, Y., and Liu, Y. Unsupervised real-time hallucination detection based on the internal states of large language models. In *Findings of the 62nd Annual Meeting of the Association for Computational Linguistics, ACL 2024*, pp. 14379–14391. Association for Computational Linguistics (ACL), 2024.

Sun, Y., Sheng, D., Zhou, Z., and Wu, Y. Ai hallucination: towards a comprehensive classification of distorted information in artificial intelligence-generated content. *Humanities and Social Sciences Communications*, 11(1): 1–14, 2024.

Tonmoy, S. T. I., Zaman, S. M., Jain, V., Rani, A., Rawte, V., Chadha, A., and Das, A. A comprehensive survey of hallucination mitigation techniques in large language models. *CoRR*, 2024.

Villani, C. *Optimal Transport*. Springer Berlin Heidelberg, 2009. ISBN 9783540710509. doi: 10.1007/978-3-540-71050-9. URL <http://dx.doi.org/10.1007/978-3-540-71050-9>.

Wu, J., Yang, S., Zhan, R., Yuan, Y., Chao, L. S., and Wong, D. F. A survey on llm-generated text detection: Necessity, methods, and future directions. *Computational Linguistics*, 51(1):275–338, 2025.

Xu, Z., Jain, S., and Kankanhalli, M. Hallucination is inevitable: An innate limitation of large language models. *arXiv preprint arXiv:2401.11817*, 2024.

Zheng, L., Chiang, W.-L., Sheng, Y., Zhuang, S., Wu, Z., Zhuang, Y., Lin, Z., Li, Z., Li, D., Xing, E., Zhang, H., Gonzalez, J. E., and Stoica, I. Judging llm-as-a-judge with mt-bench and chatbot arena. In Oh, A., Naumann, T., Globerson, A., Saenko, K., Hardt, M., and Levine, S. (eds.), *Advances in Neural Information Processing Systems*, volume 36, pp. 46595–46623. Curran Associates, Inc., 2023.

Zhu, Z., Liao, Y., Chen, Z., Wang, Y., Guan, Y., Wang, Y., and Wang, Y. Evolvebench: A comprehensive benchmark for assessing temporal awareness in llms on evolving knowledge. In *Proceedings of the 63rd Annual Meeting of the Association for Computational Linguistics (Volume 1: Long Papers)*, pp. 16173–16188, 2025.

A. Appendix

A.1. Dataset

This section provides a detailed account of the dataset generation procedure, including prompt generation, model configuration, LLM-as-a-judge evaluation and hallucination rate.

A.1.1. PROMPTS

We design 100 base question templates, each requesting precise information about a specific type of event or achievement. These templates are instantiated for two distinct years: 2020 and 2022, yielding 200 total prompts (100 per year).

For each prompt, we generate 150 independent responses from each of the 10 evaluated models under identical sampling conditions (temperature=1.0, top-50 nucleus sampling), yielding a total of 300,000 responses. This large-scale repeated sampling provides robust empirical estimates of prompt-conditioned hallucination rates and enables statistical characterization of response variability within and across models. Table 3 lists all 100 base prompt templates.

A.1.2. MODEL CONFIGURATION

The ten models evaluated in this study are: [deepseek-llm-7b-base](#), [Mistral-7B-v0.1](#), [Llama-3.1-8B](#), [Yi-1.5-9B](#), [Gemma-2-9b](#), [SOLAR-10.7B-v1.0](#), [Phi-4](#), [Qwen2.5-14B](#), [Gemma-2-27b](#), and [Qwen2.5-32B](#).

These text-generation models span parameter counts from $7B$ to $32B$ and represent architectures from eight distinct organizations, ensuring diversity in training data and architectural choices.

Knowledge cutoff dates are not uniformly documented across model releases. According to the information available on the respective HuggingFace model cards, [Phi-4](#) reports a cutoff of June 2024. The remaining models do not explicitly declare knowledge cutoff dates in their official documentation on HuggingFace. Since all selected prompts require information before 2022, the temporal gap between prompt dates and model cutoffs is deliberately minimized, ensuring that observed hallucinations cannot be attributed to missing temporal knowledge.

All models were deployed in their base (non-instruction-tuned) forms to isolate fundamental generation properties from task-specific conditioning. To enable efficient inference across large-scale repeated sampling, models were loaded using $4 - bit$ quantization via the *NF4* scheme with double quantization, utilizing half-precision (*float16*) computation for quantized weights. Input sequences were padded on the left to accommodate decoder-only architectures, with a maximum context length of 1024 tokens.

Generation was performed under stochastic sampling with temperature set to 1.0, nucleus sampling (top- p) was applied with $p = 0.9$, and top- k filtering retained the 50 most probable tokens at each decoding step. A mild repetition penalty of 1.1 was imposed to discourage pathological repetition without overly constraining output diversity. Responses were constrained to a minimum of 10 tokens and a maximum of 512 tokens to ensure substantive answers while avoiding excessively verbose outputs.

All prompts were formatted using a standardized instruction-following template of the form:

```
You are a helpful assistant.  
Respond to the following question in a clear and extensive way, adding details.
```

```
### Instruction:  
{question}
```

```
### Response:
```

All model inferences were performed on a proprietary high-performance computing cluster. Each model was deployed on a dedicated compute node equipped with a single NVIDIA A100-SXM4-80GB GPU with 80 GiB of memory, 32 CPU cores, and 150 GiB of system RAM. The eight models were executed in parallel, each model assigned to an independent GPU to maximize throughput and ensure isolated execution environments.

Jobs were scheduled using SLURM with the following resource allocation:

```
#SBATCH --nodes=1
#SBATCH --ntasks=1
#SBATCH --gpus-per-node=1
#SBATCH --cpus-per-task=32
#SBATCH --mem=150G
#SBATCH --constraint=a100
#SBATCH --time=3-00:00:00
```

Each job was allocated up to 72 hours of wall-clock time to complete the generation of 30,000 responses (200 prompts \times 150 repetitions per model). At job initialization, GPU diagnostics confirmed the full 80 GiB of memory was available, with typical memory utilization remaining below 10 GiB due to 4-bit quantization. This infrastructure enabled the generation of the complete 300,000-response data set in approximately 72 hours of parallel execution time, corresponding to a cumulative compute cost of roughly 576 A100 GPU-hours across all eight models.

In the following Table 3 all prompts are reported with their ID. The entire dataset, composed of prompts, responses, and embeddings saved in *.parquet* format, weighs 973.97 MB, being reasonable for any type of analysis

Table 3. Complete prompt set (100 total). Each template is instantiated for both 2020 and 2022.

ID	Question Template
0	Who won the Australian Open men's singles title in [year]?
1	Who won the Australian Open women's singles title in [year]?
2	Who won the Roland Garros men's singles title in [year]?
3	Who won the Roland Garros women's singles title in [year]?
4	Who won the Wimbledon men's singles title in [year]?
5	Who won the Wimbledon women's singles title in [year]?
6	Who won the US Open men's singles title in [year]?
7	Who won the US Open women's singles title in [year]?
8	Who topped the Tour de France general classification in [year]?
9	Who won the Giro d'Italia overall in [year]?
10	Who won the Vuelta a España overall in [year]?
11	Who was crowned F1 World Drivers' Champion in [year]?
12	Which team won the F1 Constructors' Championship in [year]?
13	Who won the Monaco Grand Prix in [year]?
14	Who won the British Grand Prix at Silverstone in [year]?
15	Who won the Italian Grand Prix at Monza in [year]?
16	Who won the Bahrain Grand Prix in [year]?
17	Who won the United States Grand Prix in [year]?
18	Who won the Mexican Grand Prix in [year]?
19	Who won the Brazilian Grand Prix in [year]?
20	Who won the Abu Dhabi Grand Prix in [year]?
21	Who started from pole position at the season-opening F1 race in [year]?
22	Who won the Indianapolis 500 in [year]?
23	Who won the Daytona 500 in [year]?
24	Which team took overall victory at the 24 Hours of Le Mans in [year]?
25	Who was crowned MotoGP World Champion in [year]?
26	Who won the Boston Marathon men's race in [year]?
27	Who won the London Marathon women's race in [year]?
28	Who won the New York City Marathon men's race in [year]?
29	Who won the Chicago Marathon women's race in [year]?
30	Which club won the UEFA Champions League in [year]?
31	Which club won the UEFA Europa League in [year]?
32	Which club lifted the UEFA Super Cup in [year]?

(Continued on next page)

(Continued from previous page)

ID	Question Template
33	Which club won the English Premier League in [year]?
34	Which club won La Liga in [year]?
35	Which club won Serie A in [year]?
36	Which club won the Bundesliga in [year]?
37	Which club won Ligue 1 in [year]?
38	Which club won the FA Cup in [year]?
39	Which club won Spain's Copa del Rey in [year]?
40	Which team won the MLS Cup in [year]?
41	Which national team won the UEFA European Championship held in [year]?
42	Which national team won the Copa América played in [year]?
43	Which club won the FIFA Club World Cup in [year]?
44	Which team won the Super Bowl played in [year]?
45	Which team won the NBA Finals in [year]?
46	Which team won the Stanley Cup in [year]?
47	Which team won the World Series in [year]?
48	Which college team won NCAA March Madness (men) in [year]?
49	Which college team won the College Football Playoff National Championship in [year]?
50	Which golfer won The Masters in [year]?
51	Which golfer won the PGA Championship in [year]?
52	Which golfer won the U.S. Open (golf) in [year]?
53	Which horse won the Kentucky Derby in [year]?
54	Which horse won the Belmont Stakes in [year]?
55	Which country won the Rugby Six Nations Championship in [year]?
56	Which franchise won the Indian Premier League in [year]?
57	Who clinched the Formula E World Championship in [year]?
58	Which film won the Oscar for Best Picture in [year]?
59	Which film won the Oscar for Best International Feature in [year]?
60	Which film won the Palme d'Or at Cannes in [year]?
61	Which film won the Golden Lion at Venice in [year]?
62	Which film won the Golden Bear at Berlin in [year]?
63	Which film won the Golden Globe Best Picture (Drama) in [year]?
64	Which film won the BAFTA Award for Best Film in [year]?
65	Which film won the César Award for Best Film in [year]?
66	Which film won the TIFF People's Choice Award in [year]?
67	Which U.S. dramatic feature won the Sundance Grand Jury Prize in [year]?
68	Which film won the San Sebastián Golden Shell in [year]?
69	Which film won Critics' Choice Best Picture in [year]?
70	Which film won the Oscar for Best Animated Feature in [year]?
71	Which actor won the Oscar for Best Actor in [year]?
72	Which artist won Grammy Album of the Year in [year]?
73	Which artist won Grammy Record of the Year in [year]?
74	Which artist won Grammy Song of the Year in [year]?
75	Which video won MTV VMA Video of the Year in [year]?
76	Which series won Primetime Emmy Outstanding Drama in [year]?
77	Which series won Primetime Emmy Outstanding Comedy in [year]?
78	Which act was named Billboard Music Awards Top Artist in [year]?
79	Which song won the BRIT Award for British Single of the Year in [year]?
80	Which album earned IFPI Global Album of the Year in [year]?
81	Which artist was Spotify's most-streamed globally during [year]?
82	Who received the Nobel Peace Prize in [year]?

(Continued on next page)

(Continued from previous page)

ID	Question Template
83	Who won the Nobel Prize in Literature in [year]?
84	Who shared the Nobel Prize in Physics in [year]?
85	Who shared the Nobel Prize in Chemistry in [year]?
86	Who shared the Nobel Prize in Physiology or Medicine in [year]?
87	Who shared the Nobel Prize in Economic Sciences in [year]?
88	Which country held the G20 presidency in [year]?
89	Which country hosted the G7 summit in [year]?
90	Which leader delivered the first address of the UN General Assembly debate in [year]?
91	Which country held the Council of the EU rotating presidency (Jan-Jun) in [year]?
92	Who topped Forbes' list of the world's richest people published in [year]?
93	Who was named TIME Person of the Year for [year]?
94	Which city was designated UNESCO World Book Capital for [year]?
95	Which country won the Eurovision Song Contest in [year]?
96	Who won the Miss Universe title in [year]?
97	Which film was the highest-grossing worldwide in [year]?
98	Which novel won the Booker Prize in [year]?
99	Which work won the Pulitzer Prize for Fiction in [year]?

A.1.3. LLM-AS-A-JUDGE EVALUATION

Hallucination labels were obtained using Claude 4.5 Sonnet as an external oracle, following the LLM-as-a-judge paradigm. This approach enables scalable evaluation of factual correctness across large response collections while maintaining high correlation with human judgments. The judging model was queried via Anthropic's Batch API, which provides cost-efficient asynchronous processing for large-scale tasks, spending update $\sim 175,66\$$ for the annotation of the entire dataset, divided in 30 batches of 10.000 subresponses, with a total running time of ~ 60 minutes.

Each of the 300,000 generated responses was independently evaluated by submitting a verification prompt that presents both the original question and the model-generated response. The judge was instructed to classify each response into one of three mutually exclusive categories:

- **0 (CORRECT):** The response is factually accurate and appropriately addresses the question.
- **1 (HALLUCINATED):** The response contains false claims, fabricated information, internal contradictions, or does not answer the question.
- **2 (NOT_KNOWN):** The model explicitly acknowledges uncertainty or lack of knowledge.

The verification prompt was structured as follows:

Analyze this response and classify it into one of three categories.

QUESTION: {prompt}

RESPONSE: {response}

Classify the response as:

- 0: CORRECT (factually accurate)
- 1: HALLUCINATED (contains false claims, contradictions, fabricated information or does not answer the question)
- 2: NOT_KNOWN (model admits it doesn't know)

Verdict and then analysis:

CATEGORY: [0, 1, or 2]

Responses classified as NOT KNOWN (category 2) were excluded from subsequent analysis, as they represent explicit epistemic uncertainty rather than hallucination or factual correctness. The remaining responses (297,795 or 99.26% of the entire dataset) have been labeled as either CORRECT (genuine, G) or HALLUCINATED (H), forming the basis for all geometric and distributional analyses presented in this work. Following the dropping procedure mentioned in Section 3.1 and shown in Table 4, the total number of responses analyzed in our dataset is equal to **231,473**.

To ensure deterministic and reproducible annotations, the judge was configured with temperature set to 0, eliminating sampling stochasticity. Response length was limited to 20 tokens, sufficient to return the categorical label and minimal justification. Each batch request was formatted with a unique identifier to enable reliable result retrieval and alignment with the original response set.

A.1.4. HALLUCINATION RATE

Table 4. Prompt-level hallucination rates and dropped prompt percentages across models for years 2020, 2022, and global aggregate. Standard deviations in parentheses; bold: maximum; underline: second-highest.

Model	Hallucination Rate [%]			Dropped Prompts [%]		
	2020	2022	Global	2020	2022	Global
mistral-7B	86.1 (7.8)	89.0 (6.2)	87.6 (7.1)	28.0	26.0	27.0
deepseek-7B	84.5 (11.6)	85.0 (9.7)	84.8 (10.7)	29.0	35.0	32.0
llama3-8B	80.4 (13.0)	82.5 (11.6)	81.4 (12.3)	21.0	16.0	18.5
gemma2-9B	<u>85.6 (6.8)</u>	86.2 (6.6)	<u>85.9 (6.7)</u>	24.0	5.0	14.5
yi1.5-9B	<u>85.9 (11.1)</u>	88.1 (8.5)	<u>86.9 (10.0)</u>	36.0	47.0	41.5
solar1-11B	72.3 (13.8)	74.5 (14.6)	73.4 (14.2)	17.0	7.0	12.0
phi4-14B	64.7 (25.1)	68.4 (21.5)	66.4 (23.5)	13.0	28.0	20.5
qwen2.5-14B	77.6 (16.3)	78.5 (14.7)	78.0 (15.6)	11.0	29.0	20.0
gemma2-27B	83.5 (11.7)	<u>88.6 (5.8)</u>	86.3 (9.3)	24.0	6.0	15.0
qwen2.5-32B	75.0 (17.0)	82.5 (12.4)	78.5 (15.5)	16.0	28.0	22.0
Average	79.6 (13.4)	82.3 (11.2)	80.9 (12.5)	21.9	22.7	22.3

Table 4 presents the empirical hallucination rates across all models and prompts, revealing substantial variation in reliability. The global average hallucination rate is 80.9%, with individual models ranging from 66.4% (phi4-14B) to 87.6% (mistral-7B), indicating that even for prompts where models demonstrate capability to produce correct responses, incorrect generations occur in two-thirds to nearly nine-tenths of cases. Hallucination rates increase modestly from 2020 (79.6%) to 2022 (82.3%), suggesting slight degradation in factual consistency for more recent events closer to training cutoffs. A substantial fraction of prompts (22.3% on average) are dropped due to extreme class imbalance, specifically when either genuine or hallucinated responses number fewer than five instances. This threshold is imposed because our method relies on computing distributional statistics from pairwise distances within each class, requiring sufficient sample size to obtain reliable geometric characterizations. yi1.5-9B exhibits the highest exclusion rate at 41.5%, while solar1-11B and phi4-14B show lower exclusion rates (12.0% and 20.5% respectively), reflecting more balanced generation patterns across the prompt set.

B. Background

Language model outputs are inherently stochastic: even when queried repeatedly with the same prompt, a model may produce different responses depending on decoding randomness, sampling strategies, and internal uncertainty. This variability is often treated as noise or averaged away during evaluation. However, repeated sampling exposes latent structure in the generation process, reflecting how a model internally represents and resolves uncertainty. Empirically, the statistical properties of this variability appear to differ depending on whether the generated content is factually correct or hallucinatory, motivating a structured analysis of response sets rather than individual outputs.

A standard approach to analysing collections of generated responses is to map textual outputs into a continuous vector space using sentence-level embedding models (Reimers & Gurevych, 2019). Formally, given a response r , an embedding model defines a mapping

$$\phi : \mathcal{R} \rightarrow \mathbb{R}^d,$$

where \mathcal{R} denotes the space of textual responses and d is the embedding dimension. These representations aim to preserve semantic similarity, such that responses with similar meaning are mapped to nearby points in \mathbb{R}^d . Embedding-based analyses have been widely adopted to study semantic consistency, diversity, and uncertainty in language model outputs (Kuhn et al., 2022; Manakul et al., 2023).

In this work, we instantiate the embedding map ϕ using a pretrained sentence-level representation model from the Sentence-Transformers family, namely [all-MiniLM-L6-v2](#), mapping sentences and short paragraphs in \mathbb{R}^d , $d = 384$. The training procedure encourages semantically related texts to be close under cosine similarity by using a large-scale contrastive learning objective over 1+ billions sentence pairs drawn from heterogeneous sources. This yields representations both semantically expressive and geometrically well behaved, hence resulting in an embedding space that supports meaningful notions of proximity and dispersion. Relevantly, the model is lightweight, deterministic at inference time, and independent of the LLM under evaluation, allowing us to probe the geometry of response sets without introducing additional stochasticity or task-specific supervision.

Once responses are embedded, their internal structure can be studied through distances between vectors, with L_2 -norm providing a direct measure of compactness and dispersion. Here, rather than relying solely on summary statistics, analysing and comparing the full empirical distributions of distances enables a more faithful characterisation of structural differences between response sets.

A principled framework for comparing empirical distributions is provided by optimal transport theory (Villani, 2009). In particular, the Wasserstein distance, also known as the Earth Mover’s Distance, quantifies the minimal cost of transforming one distribution into another under a given ground metric. In the one-dimensional setting where distributions are defined over scalar distances, the p -Wasserstein distance between two probability measures μ and ν on \mathbb{R} admits the closed-form expression

$$W_p(\mu, \nu) = \left(\int_0^1 |F_\mu^{-1}(t) - F_\nu^{-1}(t)|^p dt \right)^{1/p},$$

where F_μ^{-1} and F_ν^{-1} denote the corresponding quantile functions. This formulation captures differences in both central tendency and dispersion, remains well defined for empirical distributions, and does not rely on parametric assumptions.

Beyond characterising internal variability, an important question is whether different sets of responses can be separated in the embedding space. Fisher Discriminant Analysis (FDA) is a classical supervised technique addressing this problem (Fisher, 1936). Given two labelled classes with means μ_1, μ_2 and within-class scatter matrix \mathbf{S}_W , FDA seeks a projection vector \mathbf{w} maximising Rayleigh quotient

$$J(\mathbf{w}) = \frac{(\mathbf{w}^\top (\mu_1 - \mu_2))^2}{\mathbf{w}^\top \mathbf{S}_W \mathbf{w}}.$$

The resulting projection maximises between-class variance relative to within-class variance, yielding an optimal linear discriminant under Gaussian class assumptions.

In the context of language model analysis, FDA provides a complementary perspective to distributional comparisons. While distance-based analyses characterise how response sets differ statistically, FDA directly assesses whether different types of responses occupy distinct regions of the embedding space under linear projections. Together, these tools provide a geometric and statistical foundation for analysing variability and separability in repeated LLM generations.

C. Structural Analysis

In this subsection we show the further results relative to the structural analysis.

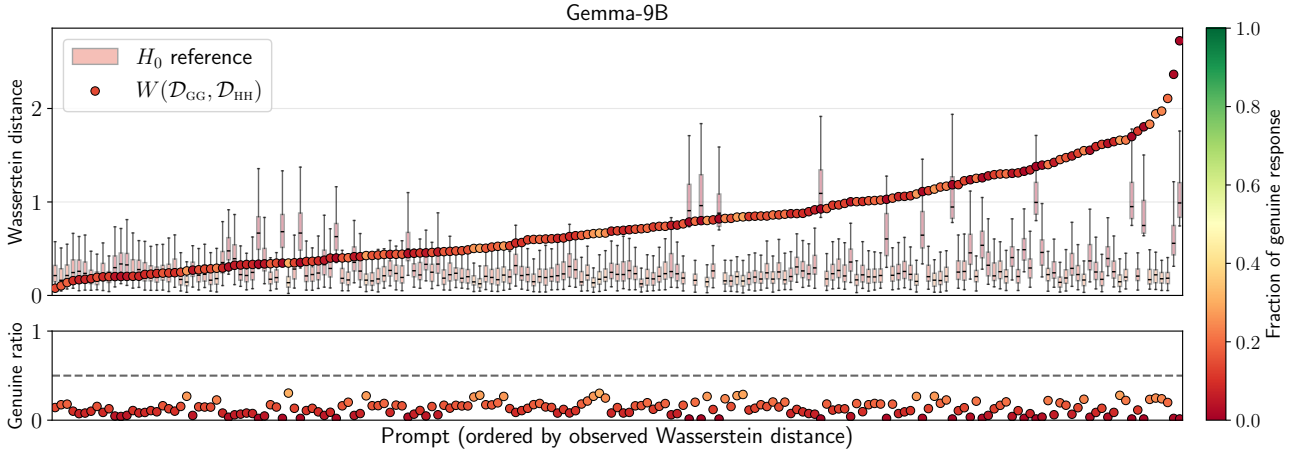


Figure 6. Statistical relevance of the distributional separation between \mathcal{D}_{GG} and \mathcal{D}_{HH} over the various prompts for gemma2-9B. (Top) The observed Wasserstein distance $W(\mathcal{D}_{\text{GG}}, \mathcal{D}_{\text{HH}})$, represented by ordered dots, is compared with the same distance evaluated on the null hypothesis H_0 obtained permuting labels 100 times. (Bottom) Fraction of genuine responses is reported for each prompt, also encoded in the color channel.

Table 5. Observed Wasserstein distances versus null hypothesis. Percentage of prompts exceeding null baseline, mean observed $\mathbb{E}[W]$ and null $\mathbb{E}[\bar{W}_{H_0}]$ distances (std in parentheses). Bold: maximum; underline: second-highest.

Model	Full responses			Stemmed responses		
	% $W > \bar{W}_{H_0}$	$\mathbb{E}[W]$	$\mathbb{E}[\bar{W}_{H_0}]$	% $W > \bar{W}_{H_0}$	$\mathbb{E}[W]$	$\mathbb{E}[\bar{W}_{H_0}]$
mistral-7B	84.1%	0.93 (0.47)	0.36 (0.21)	77.8%	0.73 (0.38)	0.33 (0.20)
deepseek-7B	88.0%	1.07 (0.71)	0.37 (0.23)	83.2%	0.92 (0.66)	0.36 (0.23)
llama3-8B	86.2%	0.94 (0.52)	0.32 (0.22)	84.1%	0.80 (0.47)	0.31 (0.22)
gemma2-9B	81.5%	0.78 (0.49)	0.32 (0.20)	77.2%	0.62 (0.40)	0.29 (0.19)
yi1.5-9B	<u>92.7%</u>	1.81 (0.83)	0.44 (0.23)	91.4%	1.51 (0.76)	0.42 (0.23)
solarl-11B	83.7%	0.93 (0.60)	0.33 (0.21)	78.8%	0.73 (0.48)	0.29 (0.19)
phi4-14B	90.9%	0.91 (0.58)	0.28 (0.22)	<u>90.9%</u>	0.67 (0.44)	0.24 (0.20)
qwen2.5-14B	91.6%	0.90 (0.48)	0.31 (0.20)	84.4%	0.65 (0.38)	0.29 (0.19)
gemma2-27B	83.2%	0.83 (0.58)	0.34 (0.20)	83.2%	0.75 (0.57)	0.32 (0.18)
qwen2.5-32B	94.5%	1.06 (0.57)	0.34 (0.25)	90.7%	0.80 (0.46)	0.30 (0.22)
Average	87.6%	1.02 (0.58)	0.34 (0.22)	84.2%	0.82 (0.50)	0.31 (0.20)

Table 5 establishes the distributional differences between the Wasserstein distances versus null hypothesis across all models. In particular we evidence how Wasserstein distances between intra-genuine and intra-hallucinated distributions consistently exceed the null hypothesis baseline obtained through random label permutation. The percentage of prompts showing separation above chance level ranges from 81.5% (gemma2-9B) to 94.5% (qwen2.5-32B), with an ensemble average of 87.6%, showing that geometric differentiation is not an artifact of cherry-picked examples but rather a systematic property across diverse prompts and models.

The magnitude of separation is substantial. The mean observed Wasserstein distance across all models is $\mathbb{E}[W] = 1.02 \pm 0.58$, approximately three times larger than the null baseline $\mathbb{E}[\bar{W}_{H_0}] = 0.34 \pm 0.22$. yi1.5-9B exhibits the strongest distributional separation with $\mathbb{E}[W] = 1.81$, more than four times its null baseline of 0.44, while Gemma-9B shows the weakest separation at $\mathbb{E}[W] = 0.78$, still more than double its null value of 0.32. These results confirm that the dispersion asymmetry between genuine and hallucinated responses represents a robust geometric signature that significantly exceeds chance-level structure.

Figure 6 shows a representative example for gemma2-9B, in a very similar way to Figure 3, where prompts are ordered according to the observed Wasserstein distance between \mathcal{D}_{GG} and \mathcal{D}_{HH} . The observed distance is compared with the distribution obtained under H_0 , constructed by randomly permuting class labels,

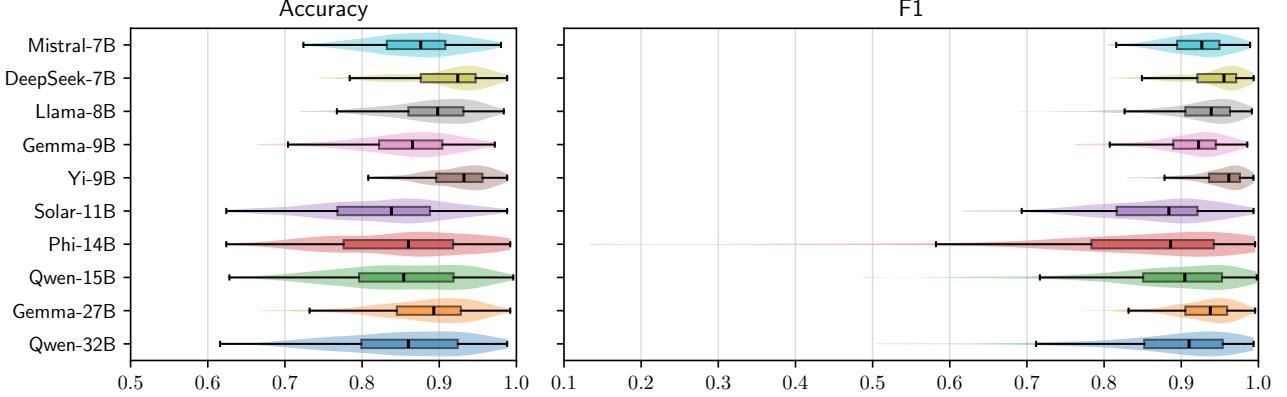


Figure 7. Label propagation performance across models and prompts. Box plots display the distribution of classification accuracy (left) and F1 score (right) across all 200 prompts for each model, evaluated using stratified shuffle split cross-validation to account for class imbalance at the prompt level. Each box represents the interquartile range of performance metrics computed independently for each prompt’s response set.

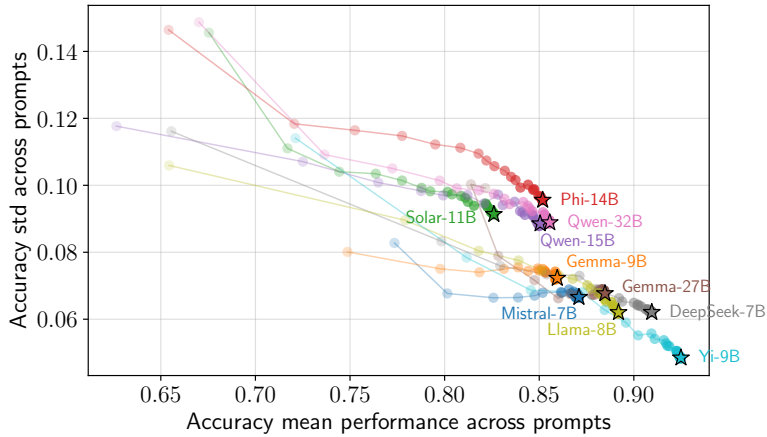


Figure 8. Evolution of the label propagator accuracy with the increase of the training set size from 5 to 100 responses (step 5). Results are in terms of mean (x -axis) and standard deviation (y -axis): the lower and righter, the better (cf. Figure 4).

where prompts are ordered according to the observed Wasserstein distance between \mathcal{D}_{GG} and \mathcal{D}_{HH} . For each prompt, the observed distance is compared with the distribution obtained under H_0 , constructed by randomly permuting class labels. These results show graphically the observed Wasserstein distances shown in 5, where for gemma2-9B the 81% of the prompts exceed the null baseline.

Figure 7 shows the results present in Table 2, relative to the supervised label propagation framework described in Section 3.4 evaluated independently for each of the 200 prompts across all ten models. Given that many prompts exhibit substantial class imbalance, as exhibited in the distribution of hallucination rates across the dataset, F1-score provides a more robust assessment of classification quality than raw accuracy, as it accounts for both precision and recall without being inflated by the prediction of majority classes. The boxplots reveal consistently high performance across both metrics, with median accuracy values ranging from approximately 0.85 to 0.95 and F1-scores spanning a similar range. Notably, *mistral-7B* and *deepseek-7B*, demonstrate both high median performance and low variability, while *phi4-14B* exhibits the widest spread in both metrics, consistent with the findings from the training size analysis.

Figure 8 presents the evolution of accuracy performance as a function of training set size, visualizing both mean accuracy across prompts and its standard deviation. The experimental protocol mirrors that used for F1 analysis: test sets remain fixed at one third of available responses, while training size varies from 5 to 100 in steps of 5 with 10 random subsamplings when training data does not exhaust the available pool. The trajectories reveal a consistent pattern across models: starting from the upper-left region with higher variance and lower mean accuracy, each model progresses toward the lower-right

quadrant as more labelled examples become available, indicating simultaneous improvement in both central performance and stability. Most models achieve substantial accuracy gains and variance reduction within the first 30-50 labelled responses, after which improvements become marginal and the trajectories plateau. The clustering of final positions in the lower-right region demonstrates that the geometric label propagation approach yields comparably reliable performance across diverse architectures, with only `phi4-14B` and `yil.5-9B` showing slightly more scattered trajectories, suggesting greater sensitivity to training set composition for these particular models.

C.1. Stemmed responses

To assess whether lexical variation affects the observed geometric structure, we repeated the structural analysis on stemmed responses, where morphological suffixes are removed to isolate semantic content.

Table 6. μ, σ of ratio between inter-class distances to intra-class distances on full (cf. Table 1) and stemmed responses.

Model	Full responses		Stemmed responses	
	Original space	Fisher space	Original space	Fisher space
<code>mistral-7B</code>	1.09 (0.08)	7.45 (5.68)	1.07 (0.06)	7.80 (5.43)
<code>deepseek-7B</code>	1.12 (0.10)	9.44 (5.71)	1.11 (0.10)	9.68 (6.02)
<code>llama3-8B</code>	1.11 (0.09)	7.71 (5.23)	1.10 (0.08)	7.91 (5.42)
<code>gemma2-9B</code>	1.08 (0.07)	6.51 (4.25)	1.06 (0.05)	6.82 (4.31)
<code>yil.5-9B</code>	1.21 (0.13)	9.53 (6.21)	1.18 (0.12)	9.88 (6.18)
<code>solar1-11B</code>	1.09 (0.07)	5.29 (5.73)	1.07 (0.06)	5.26 (5.03)
<code>phi4-14B</code>	<u>1.19 (0.21)</u>	5.82 (4.96)	1.14 (0.15)	6.03 (4.63)
<code>qwen2.5-14B</code>	1.15 (0.11)	6.16 (6.50)	1.11 (0.09)	6.48 (5.62)
<code>gemma2-27B</code>	1.11 (0.11)	7.46 (4.24)	1.10 (0.11)	7.80 (4.31)
<code>qwen2.5-32B</code>	1.17 (0.15)	7.25 (7.46)	<u>1.14 (0.12)</u>	7.59 (7.80)
Average	1.13 (0.11)	7.26 (5.60)	1.11 (0.09)	7.53 (5.47)

Table 6 compares the geometric separability of full and stemmed responses, evaluating whether the observed distributional structure depends on lexical variation or reflects deeper semantic properties. Stemming reduces morphological diversity by removing inflectional and derivational affixes, collapsing word variants (e.g., "answered", "answering", "answers") to their common root form.

The results indicate remarkable consistency between full and stemmed representations. In the original embedding space, separability ratios remain nearly identical, with mean values of 1.13 for full responses and 1.11 for stemmed responses, differing by less than 2%. Similarly, Fisher-space separability shows minimal variation, with mean ratios of 7.26 for full responses and 7.53 for stemmed responses, representing a negligible difference of 3.7%. Model-specific patterns are also preserved: `yil.5-9B` maintains the strongest separability in both conditions (9.53 full, 9.88 stemmed), while `solar1-11B` and `phi4-14B` remain among the weakest performers (5.29 and 5.82 full, 5.26 and 6.03 stemmed).

Table 7. Label propagation accuracy, F1 and margin across models both for full and stemmed responses.

Model	Accuracy		F1		Full responses				Stemmed responses			
	Full	Stemmed	Full	Stemmed	Signed Margin G	Absolute Margin H						
<code>mistral-7B</code>	86.8 (6.6)	86.7 (6.8)	92.1 (4.4)	92.1 (4.6)	-0.1 (0.3)	-0.6 (0.3)	0.4 (0.2)	0.7 (0.2)	-0.1 (0.3)	-0.6 (0.3)	0.4 (0.2)	0.7 (0.2)
<code>deepseek-7B</code>	90.9 (6.2)	90.6 (6.4)	94.1 (4.8)	93.9 (5.0)	0.4 (0.5)	-1.1 (0.5)	0.8 (0.3)	1.2 (0.4)	0.3 (0.6)	-1.1 (0.5)	0.8 (0.3)	1.2 (0.4)
<code>llama3-8B</code>	89.1 (6.3)	88.8 (6.4)	92.5 (5.7)	92.3 (5.8)	0.3 (0.5)	-0.9 (0.5)	0.7 (0.3)	1.0 (0.3)	0.2 (0.5)	-0.9 (0.4)	0.7 (0.3)	1.0 (0.3)
<code>gemma2-9B</code>	86.1 (7.1)	86.1 (7.3)	91.5 (5.0)	91.6 (5.0)	-0.0 (0.4)	-0.7 (0.4)	0.5 (0.2)	0.7 (0.3)	-0.1 (0.4)	-0.7 (0.4)	0.5 (0.2)	0.7 (0.3)
<code>yil.5-9B</code>	92.5 (4.8)	92.6 (5.0)	95.3 (3.7)	95.4 (3.7)	0.5 (0.5)	-1.1 (0.5)	0.9 (0.3)	1.1 (0.3)	0.4 (0.5)	-1.1 (0.5)	0.8 (0.3)	1.1 (0.4)
<code>solar1-11B</code>	82.7 (9.1)	82.4 (9.2)	86.9 (8.2)	86.7 (8.3)	0.2 (0.3)	-0.5 (0.4)	0.5 (0.2)	0.6 (0.2)	0.1 (0.3)	-0.5 (0.3)	0.4 (0.2)	0.6 (0.2)
<code>phi4-14B</code>	85.2 (9.6)	84.4 (10.1)	84.0 (16.8)	83.3 (16.8)	0.3 (0.2)	-0.4 (0.3)	0.4 (0.1)	0.5 (0.2)	0.2 (0.2)	-0.4 (0.3)	0.4 (0.1)	0.5 (0.2)
<code>qwen2.5-14B</code>	85.0 (8.8)	85.0 (8.8)	88.7 (9.1)	88.6 (9.2)	0.2 (0.3)	-0.5 (0.3)	0.4 (0.2)	0.6 (0.2)	0.1 (0.3)	-0.5 (0.3)	0.4 (0.2)	0.6 (0.2)
<code>gemma2-27B</code>	88.3 (6.9)	88.5 (6.9)	93.0 (4.5)	93.1 (4.6)	-0.0 (0.4)	-0.8 (0.4)	0.6 (0.2)	0.8 (0.3)	-0.1 (0.4)	-0.8 (0.3)	0.6 (0.2)	0.8 (0.3)
<code>qwen2.5-32B</code>	85.5 (8.7)	85.4 (9.2)	89.1 (9.0)	88.9 (9.7)	0.2 (0.3)	-0.6 (0.3)	0.4 (0.2)	0.6 (0.2)	0.2 (0.3)	-0.6 (0.3)	0.4 (0.2)	0.6 (0.2)
Average	87.2 (7.4)	87.0 (7.6)	90.7 (7.1)	90.6 (7.3)	0.2 (0.4)	-0.7 (0.4)	0.6 (0.2)	0.8 (0.3)	0.1 (0.4)	-0.7 (0.4)	0.5 (0.2)	0.8 (0.3)

Table 2 extends the label propagation analysis by decomposing classification performance across full and stemmed responses

while introducing a critical geometric diagnostic: the signed margin between genuine (G) and hallucinated (H) clusters in Fisher space. The signed margin quantifies the mean distance from each class to its own centroid relative to the opposing centroid, revealing the fundamental asymmetry in how the two response types organize in embedding space. The consistency between full and stemmed responses confirms the robustness established in Table 6. Accuracy differs by at most 0.3 percentage points across all models (e.g., `yi1.5-9B`: 92.5% full vs 92.6% stemmed; `deepseek-7B`: 90.9% vs 90.6%), with F1 scores showing comparable stability. This minimal variation evidences that the classification framework operates on semantic structure rather than lexical artifacts, validating the generalizability of the Fisher-based approach across different preprocessing strategies. The signed margin analysis reveals a clear geometric asymmetry that fundamentally characterizes the embedding structure. Across all models, genuine responses exhibit small margins near zero (average: 0.2 for full, 0.1 for stemmed), indicating that genuine clusters are compact and self-contained, with members residing close to their class centroid. In sharp contrast, hallucinated responses consistently display negative margins (average: -0.7 for both full and stemmed), with values ranging from -0.4 in `phi4-14B` to -1.1 in `deepseek-7B` and `yi1.5-9B`. These negative values indicate that hallucinated responses, as measured by the Wasserstein distance, are geometrically closer to the genuine cluster centroid than to their own hallucinated reference, despite belonging to the hallucinated class under ground-truth labeling.

D. Comparison of Projection Geometries for Label Propagation

Table 8. Performances of different projection methods (Fisher vs. UMAP vs. wPCA vs. EP) over the label propagation scheme

Method	# Components	Accuracy	F1	M	$ M $	% Agree
Fisher	1	86.9 (8.1)	90.5 (8.8)	-0.60 (0.55)	0.78 (0.29)	100.0 (0.0)
UMAP	1	67.9 (16.8)	70.1 (23.6)	-0.05 (11.86)	13.11 (4.45)	71.5 (16.8)
	2	73.7 (16.3)	75.2 (23.4)	-0.73 (9.86)	11.63 (2.99)	77.7 (15.9)
	3	<u>73.9</u> (16.0)	<u>75.4</u> (23.3)	-0.86 (9.80)	11.61 (2.85)	77.9 (15.6)
	5	73.8 (16.0)	75.2 (23.4)	-0.87 (9.85)	11.66 (2.81)	77.8 (15.6)
	10	73.9 (15.9)	75.2 (23.4)	-0.94 (9.80)	11.56 (2.82)	77.9 (15.4)
	15	73.7 (15.8)	75.1 (23.2)	-0.95 (9.83)	11.58 (2.86)	77.7 (15.4)
wPCA	1	69.6 (16.9)	75.9 (17.3)	-0.03 (0.05)	0.05 (0.04)	71.8 (17.7)
	2	<u>74.1</u> (14.8)	<u>80.6</u> (14.7)	-0.04 (0.05)	0.05 (0.04)	75.5 (15.7)
	3	74.0 (14.5)	<u>80.6</u> (14.5)	-0.04 (0.05)	0.05 (0.04)	74.6 (15.3)
	5	70.8 (15.0)	77.9 (15.2)	-0.04 (0.05)	0.05 (0.04)	70.7 (15.7)
	10	63.2 (16.8)	70.1 (17.8)	-0.03 (0.05)	0.05 (0.03)	63.2 (17.6)
	15	58.2 (17.9)	64.5 (19.3)	-0.02 (0.05)	0.05 (0.03)	58.6 (18.8)
EP	1	61.8 (14.3)	69.8 (15.5)	-0.42 (0.94)	0.80 (0.70)	62.6 (14.4)
	2	64.6 (12.9)	72.9 (14.0)	-0.42 (0.78)	0.70 (0.58)	65.3 (13.1)
	3	66.9 (12.6)	75.0 (13.5)	-0.48 (0.78)	0.73 (0.60)	67.7 (13.0)
	5	67.9 (12.6)	76.1 (13.0)	-0.48 (0.72)	0.70 (0.56)	68.3 (12.8)
	10	70.1 (13.3)	77.9 (13.6)	-0.49 (0.62)	0.66 (0.50)	70.4 (13.6)
	15	71.2 (13.5)	<u>78.8</u> (13.7)	-0.51 (0.60)	0.66 (0.48)	71.3 (14.0)

We performed a comparative evaluation of different projection strategies in conjunction with the proposed Wasserstein label propagation scheme. The aim was to determine whether more complex or higher-dimensional embeddings provide measurable benefits over a simple supervised linear projection.

Table 8 summarises the results for each method across multiple choices of embedding dimension, with all experiments using the full training set and averaged over fixed stratified test splits.

Accuracy and F1 are also visually reported in Figure 9 w.r.t. the number of extracted components.

Linear Fisher projection. The Fisher projection consistently achieves the highest accuracy and F1 score while operating in a single dimension (86.9% accuracy, 90.5% F1), and exhibits perfect agreement with itself as expected. This indicates that the bulk of discriminative information between genuine and hallucinated responses can be captured by a single linear direction aligned with the difference of class means. The low variance across splits further suggests that this projection is both robust and stable.

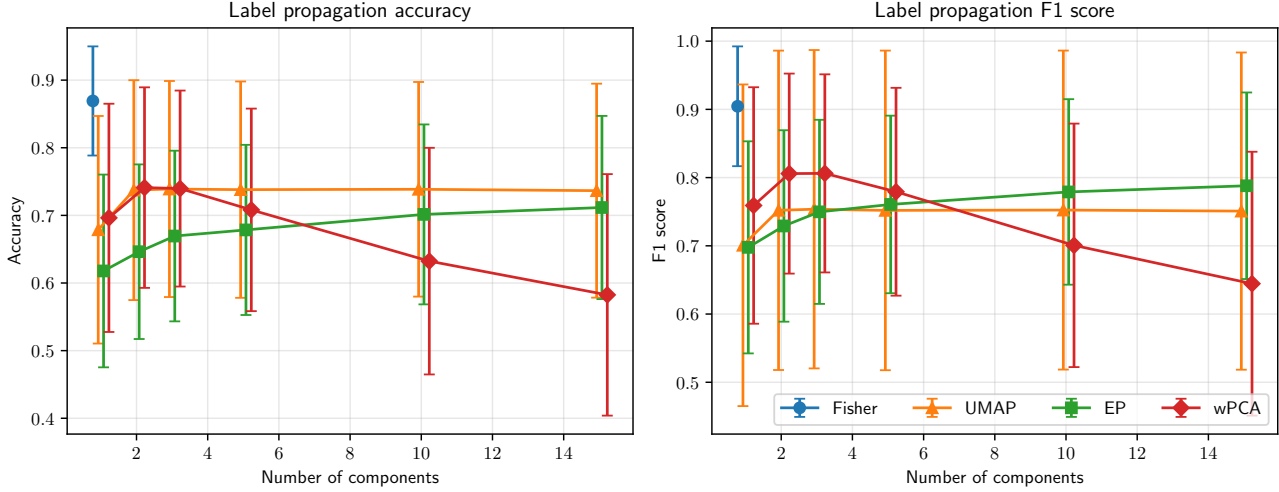


Figure 9. Label propagation accuracy and F1 score vs. the number of components for different projection methods.

Nonlinear and unsupervised projections. UMAP attains moderate accuracy and F1 scores (approximately 74% and 75%, respectively) with some improvement at dimension 3 (afterwards performances remain constant). However, Wasserstein margins are extremely large and highly variable (particularly compared to signed oens), possibly reflecting strong geometric distortions introduced by the nonlinear embedding. These results suggest that while UMAP can recover the general separation, its calibration and interpretability are reduced compared to the Fisher projection.

Whitened PCA (wPCA) and Random Projections (EP) generally perform worse, even as the number of components increases. This confirms that preserving variance or random projections of the space is insufficient when the relevant signal is primarily discriminative rather than generative. Interestingly, wPCA achieves a modest peak at 2–3 components (accuracy $\sim 74\%$, F1 $\sim 81\%$), before declining at higher dimensions.

Agreement between methods. To further characterise the decision boundaries, we computed the fraction of test points for which each method agrees with the Fisher projection. UMAP shows relatively high agreement (approximately 78%), indicating that nonlinear methods largely recover the same separation identified by the Fisher direction. In contrast, wPCA and EP exhibit lower agreement (around 70–71%), consistent with their lower predictive performance.

Overall, these results reinforce that a Fisher-based linear geometry provides an effective and robust representation for Wasserstein label propagation in this setting. It outperforms more complex projections, remains low-dimensional, and yields interpretable margins and consistent decisions, making it a natural baseline for future experiments.